Journal of Quantitative Spectroscopy & Radiative Transfer 146 (2014) 34–40

Contents lists available at ScienceDirect

Journal of Quantitative Spectroscopy & Radiative Transfer

journal homepage: www.elsevier.com/locate/jqsrt

Multiple scattering calculations for nonreciprocal planar magnetoplasmonic nanostructures

A. Christofi [a,*], C. Tserkezis [b], N. Stefanou [a]

[a] Department of Solid State Physics, University of Athens, Panepistimioupolis, GR-157 84 Athens, Greece
[b] Donostia International Physics Center (DIPC) and Centro de Física de Materiales (CFM) CSIC-UPV/EHU, Paseo Manuel de Lardizabal 5, Donostia-San Sebastián 20018, Spain

ARTICLE INFO

Article history:
Received 30 October 2013
Received in revised form
23 December 2013
Accepted 30 December 2013
Available online 11 January 2014

Keywords:
Multiple light scattering
Magnetophotonic crystals
Plasmonics
Spectral nonreciprocity
Photonic surface states

ABSTRACT

We present an extended version of the layer-multiple-scattering method, which is ideally suited for the study of photonic crystals of different kinds of particles, encompassing homogeneous and multicoated chiral and nonchiral spheres, gyrotropic spheres, as well as homogeneous nonspherical particles. The efficiency of the method is demonstrated on specific examples of planar magnetoplasmonic nanostructures that lack, simultaneously, time-reversal and space-inversion symmetries. Nonreciprocal transport of light at the (001) surface of a semi-infinite face centered cubic (fcc) crystal of plasma nanospheres under the action of an external, in-plane, static magnetic field and of surface plasmon polaritons at the surface of a plasmonic material coated with an overlayer of magnetized garnet nanospheres is demonstrated in the Voigt geometry.

1. Introduction

Spectral nonreciprocity is in principle encountered in systems that lack both space-inversion and time-reversal symmetries [1]. Nonreciprocal electromagnetic (EM) devices, such as isolators and circulators, operating at radio and microwave frequencies can be realized using ferrite materials biased by a static magnetic field, which breaks local time-reversal symmetry and induces a strong gyrotropic response. However, at infrared and visible frequencies the gyrotropic response of materials is rather weak and can be described by a relative magnetic permeability $\mu_g = 1$ and, assuming the magnetization along the z-direction, a relative electric permittivity tensor of the form

$$\overleftrightarrow{\varepsilon}_g = \begin{pmatrix} \varepsilon_r & -i\varepsilon_\kappa & 0 \\ i\varepsilon_\kappa & \varepsilon_r & 0 \\ 0 & 0 & \varepsilon_z \end{pmatrix}, \tag{1}$$

with $\varepsilon_\kappa \ll 1$. Therefore, in this case, the design of efficient miniaturized nonreciprocal optical components is much more delicate and requires a careful investigation. In this respect, the development of full electrodynamic theoretical methods that can accurately describe low-symmetry photonic architectures without space-inversion and time-reversal symmetries with reduced computational effort is of primary importance. On the other hand, combining plasmonics with magnetism offers impressive opportunities for controlling the light–matter interaction in tailored nanostructures and designing on-chip nonreciprocal optical components. Plasmons confine light in subwavelength dimensions and greatly enhance optical fields locally, which allows one to achieve a strong magneto-optic activity [2].

In this paper we present an extended version of the layer-multiple-scattering (LMS) method, a full electrodynamic computational methodology which is ideally suited for studying various configurations of nonreciprocal magnetophotonic nanostructures. The efficiency of the method is demonstrated on two specific planar architectures which lack an inversion center: A surface of a semi-infinite crystal of magnetized plasma nanospheres and a two-dimensional

* Corresponding author. Tel.: +30 210 727 6780
E-mail address: aristi@ims.demokritos.gr (A. Christofi).

0022-4073/$ - see front matter © 2014 Elsevier Ltd. All rights reserved.
http://dx.doi.org/10.1016/j.jqsrt.2013.12.020

(2D) periodic array of magnetic garnet nanospheres deposited on a homogeneous plasmonic material substrate.

2. Layer-multiple-scattering method for photonic crystals

The LMS method provides a versatile and efficient computational framework for fast full-electrodynamic calculations of the optical properties of structures consisting of successive, possibly different layers of particles arranged with the same 2D periodicity in homogeneous host materials. Here we outline the main characteristics of the method by focusing, in particular, on the way the scattering matrices of single particles and 2D periodic arrays of these particles are employed in order to calculate the complex reflection and transmission coefficients of finite stacks of such arrays, as well as the complex photonic band structure of a corresponding infinite three-dimensional (3D) crystal. In addition, by solving appropriate secular equations that involve combinations of scattering matrices, one can identify modes localized within a finite slab built as a sequence of 2D periodic arrays of particles or homogeneous layers (slab modes), or at the surface of a corresponding semi-infinite crystal (surface states). Throughout this section we try to provide a schematic, more intuitive description of the method, avoiding extensive formalism as much as possible. Details of each step can be found elsewhere [3–14].

The method proceeds by first describing a single scattering process, as shown schematically in Fig. 1. The spatial part of the electric field associated with a monochromatic EM wave of angular frequency ω with $\exp(-i\omega t)$ time dependence in a homogeneous, isotropic medium characterized by a relative electric permittivity ε and magnetic permeability μ is expanded into regular vector spherical waves about a given origin of coordinates as follows:

$$\mathbf{E}_{\rm inc}(\mathbf{r}) = \sum_{l=1}^{\infty}\sum_{m=-l}^{l}\left[\frac{i}{q}a^0_{Elm}\nabla\times j_l(qr)\mathbf{X}_{lm}(\hat{\mathbf{r}}) + a^0_{Hlm}j_l(qr)\mathbf{X}_{lm}(\hat{\mathbf{r}})\right], \quad (2)$$

where $q=\omega\sqrt{\varepsilon\mu}/c$ with c being the velocity of light in vacuum, $j_l(qr)$ are the spherical Bessel functions, which are finite everywhere, $\mathbf{X}_{lm}(\hat{\mathbf{r}})$ are the vector spherical harmonics, and a^0_{Plm}, $P=E,H$, are appropriate expansion coefficients. When the wave described by Eq. (2) impinges on a particle centered at the origin of coordinates, it is scattered by it, so that the total wave field outside the particle consists of the incident wave and a scattered wave that can

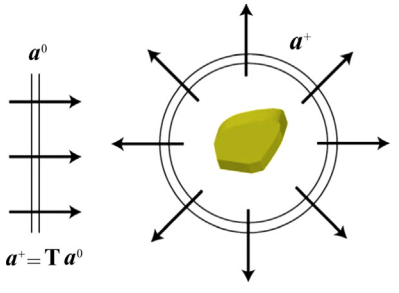

Fig. 1. Schematic representation of scattering by a single particle.

be written in the form

$$\mathbf{E}_{\rm sc}(\mathbf{r}) = \sum_{l=1}^{\infty}\sum_{m=-l}^{l}\left[\frac{i}{q}a^+_{Elm}\nabla\times h_l^+(qr)\mathbf{X}_{lm}(\hat{\mathbf{r}}) + a^+_{Hlm}h_l^+(qr)\mathbf{X}_{lm}(\hat{\mathbf{r}})\right], \quad (3)$$

where $h_l^+(qr)$ are the spherical Hankel functions that describe outgoing spherical waves: $h_l^+(qr)\approx(-i)^l\exp(iqr)/iqr$ as $r\to\infty$. Using the appropriate spherical-wave expansion for the field inside the particle and applying the usual continuity boundary conditions at the interface(s), one can express the expansion coefficients, a^+_{Plm}, of the scattered wave in terms of those of the incident wave, a^0_{Plm}, through the so-called scattering T matrix as follows:

$$a^+_{Plm} = \sum_{P'l'm'} T_{Plm;P'l'm'}a^0_{P'l'm'}. \quad (4)$$

We note that, in general, the T matrix is nondiagonal with respect to P, l and m. Only in the special case of spherical, isotropic, nonchiral particles it is a diagonal matrix, independent of m. For a homogeneous sphere it is given by the closed-form solutions of the Mie scattering problem [15]. For a sphere consisting of a number of concentric homogeneous spherical shells an analytical solution can still be derived, but it is more efficient to evaluate the T matrix using recursive algorithms [8,16,17]. For chiral homogeneous or coated spheres the T matrix is no longer diagonal with respect to P, which reflects the mixing of E- and H- polarization modes upon scattering because of chirality [9,11,18–21]. In the case of a gyrotropic sphere, the major complication arises due to the fact that, at a given frequency, the multipole expansion of the EM field inside the sphere involves vector spherical waves of different wave numbers. These wave numbers and the associated expansion coefficients are given by the eigenvalues and eigenvectors of a matrix that involves only the elements of the corresponding relative electric permittivity tensor and angular momentum numbers. Following this approach, which has been elaborated by different authors [12–14], we finally obtain a block-diagonal T matrix in the given spherical-wave representation from a set of coupled linear equations that relate the expansion coefficients of the scattered field to those of the incident field. Finally, for nonspherical scatterers no analytic solution exists and the T matrix needs to be calculated numerically. This can be done by employing the extended boundary condition method [22–24], properly adapted to the LMS formalism [6]. As a future step, and in order to further generalize the LMS method, the so-called invariant imbedding T-matrix approach, which treats irregular and inhomogeneous particles as multi-layered inhomogeneous spheres and proceeds by computing the T matrix recursively from the inscribed sphere to the circumscribed sphere [25–27], can be straightforwardly implemented into the method. It is worth noting that, in all of the above cases, a local dielectric function is assumed for the individual scatterers, though nonlocal behavior can also be treated in special cases [28].

When particles are assembled in a plane, say the $x-y$ plane, multiple scattering takes place and the wave impinging on a given particle "i" is the sum of the externally incident wave, described by expansion coefficients a^0_{Plm}, plus

the waves scattered by all the other particles, described by expansion coefficients $b^{+i'}_{P'l'm'}$. The latter produce a secondary wave incident on the i-th particle with expansion coefficients

$$b^{0i}_{Plm} = \sum_{i'} \sum_{P'l'm'} \Omega^{ii'}_{Plm;P'l'm'} b^{+i'}_{P'l'm'}, \tag{5}$$

where $\Omega^{ii'}_{Plm;P'l'm'}$ are proper propagator functions in the host medium ($\Omega^{ii'}_{Plm;P'l'm'} \equiv 0$ for $i = i'$) [3–5]. On the other hand, the wave scattered by the i-th particle is given by the corresponding particle T matrix according to Eq. (4)

$$b^{+i}_{Plm} = \sum_{P''l''m''} T^{i}_{Plm;P''l''m''} (a^{0}_{P''l''m''} + b^{0i}_{P''l''m''}) \tag{6}$$

and, substituting Eq. (5) into Eq. (6), the following system of linear equations is obtained:

$$\sum_{i'} \sum_{P'l'm'} (\delta_{ii'}\delta_{PP'}\delta_{ll'}\delta_{mm'} - \sum_{P''l''m''} T^{i}_{Plm;P''l''m''} \Omega^{ii'}_{P''l''m'';P'l'm'}) b^{+i'}_{P'l'm'} = \sum_{P''l''m''} T^{i}_{Plm;P''l''m''} a^{0}_{P''l''m''}, \quad \forall i, P, l, m. \tag{7}$$

Solving Eq. (7) determines uniquely the total scattered field in terms of the known externally incident field, as shown schematically in Fig. 2. It should be pointed out that the above-described multiple-scattering technique is in principle exact for any particle arrangement, provided that the spheres circumscribing the individual particles do not overlap with each other. In the special case that interests us here, where the particles are arranged in 2D periodic arrays, the infinite sum over the scatterers can be efficiently evaluated numerically using Ewald summation techniques [4,5,29].

Once in-plane multiple scattering is evaluated in the given spherical-wave basis, it is convenient to change the expansion basis and treat interlayer scattering using a plane-wave basis instead. The combination of these two different basis sets is one of the key characteristics to which the LMS method owes its efficiency. Let us assume a plane wave incident on a 2D periodic array of scatterers. Due to the 2D periodicity of the structure (taken to be in the $x-y$ plane), it is convenient to write the component of the wave vector of the incident plane wave parallel to the periodic array, $\mathbf{q}_\parallel$, as $\mathbf{q}_\parallel = \mathbf{k}_\parallel + \mathbf{g}'$, where $\mathbf{k}_\parallel$, the reduced wave vector in the surface Brillouin zone (SBZ), is a conserved quantity in the scattering process and $\mathbf{g}'$ is a certain reciprocal vector of the given 2D lattice. Therefore, the wave vector of the incident wave has the form

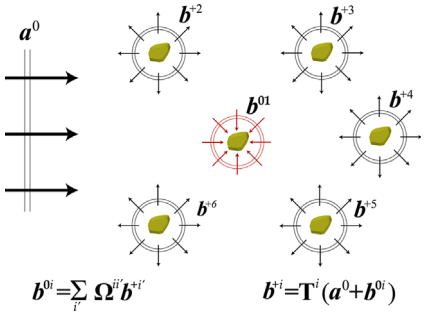

Fig. 2. Schematic representation of multiple scattering in an array of particles.

$\mathbf{K}^{\pm}_{\mathbf{g}'} = \mathbf{k}_\parallel + \mathbf{g}' \pm [q^2 - (\mathbf{k}_\parallel + \mathbf{g})^2]^{1/2} \hat{\mathbf{e}}_z$, where q is the wave number, $\hat{\mathbf{e}}_z$ is the unit vector along the z-axis, and the $+$ or $-$ sign refers to incidence from the left ($z<0$) or from the right ($z>0$), i.e., a wave propagating towards the positive or the negative direction, respectively. Since $\mathbf{k}_\parallel$ and ω are conserved quantities in the elastic scattering process, the scattered field will consist of a series of plane waves with wave vectors

$$\mathbf{K}^{\pm}_{\mathbf{g}} = \mathbf{k}_\parallel + \mathbf{g} \pm [q^2 - (\mathbf{k}_\parallel + \mathbf{g})^2]^{1/2} \hat{\mathbf{e}}_z = \mathbf{k}_\parallel + \mathbf{g} + K^{\pm}_{\mathbf{g}z} \hat{\mathbf{e}}_z, \quad \forall \mathbf{g} \tag{8}$$

and polarizations along $\hat{\mathbf{e}}_1$ and $\hat{\mathbf{e}}_2$ (polar and azimuthal unit vectors, respectively, associated with every $\mathbf{K}^{s}_{\mathbf{g}}, s = \pm$). It is worth noting that though the scattered field consists, in general, of a number of diffracted beams corresponding to different 2D reciprocal-lattice vectors $\mathbf{g}$, only beams for which $K^{\pm}_{\mathbf{g}z}$ is real constitute propagating waves. When $(\mathbf{k}_\parallel + \mathbf{g})^2 > q^2$, we have an evanescent beam and the corresponding unit vectors $\hat{\mathbf{e}}_1$, $\hat{\mathbf{e}}_2$ become complex, but they are still orthogonal: $\hat{\mathbf{e}}_p \cdot \hat{\mathbf{e}}_{p'} = \delta_{pp'}$, $p(p') = 1, 2$. The amplitudes of the transmitted and reflected plane wave beams are obtained from the amplitude of the incident plane wave as follows:

$$[E_{\mathrm{tr}}]^{+}_{\mathbf{g}p} = Q^{\mathrm{I}}_{\mathbf{g}p;\mathbf{g}'p'} [E_{\mathrm{inc}}]^{+}_{\mathbf{g}'p'}$$
$$[E_{\mathrm{rf}}]^{-}_{\mathbf{g}p} = Q^{\mathrm{III}}_{\mathbf{g}p;\mathbf{g}'p'} [E_{\mathrm{inc}}]^{+}_{\mathbf{g}'p'}, \tag{9}$$

where $\mathbf{Q}^{\mathrm{I}}$ and $\mathbf{Q}^{\mathrm{III}}$ are appropriate transmission and reflection matrices for incidence from the left, as shown schematically in Fig. 3. Similar equations hold for incidence from the right, with transmission and reflection matrices $\mathbf{Q}^{\mathrm{IV}}$ and $\mathbf{Q}^{\mathrm{II}}$, respectively [3–5].

For a composite structure consisting of several layers, the Q matrices of the individual layers can be combined so as to describe interlayer multiple scattering to any order, by including all propagating and evanescent components

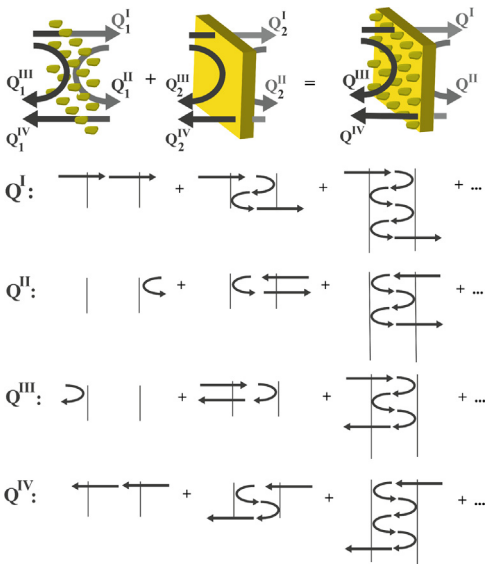

Fig. 3. The Q matrices of two successive layers are obtained from those of the individual layers, taking into account interlayer multiple scattering to any order.

of the wave field necessary to obtain convergence. In this procedure one can combine the Q matrices of layers with the same or different scatterers, and/or of homogeneous slabs, in a manner similar to the adding-doubling method used for solving radiative transfer [30,31], as shown schematically in Fig. 3. The only limitation is $\mathbf{k}_\parallel$ conservation, which is ensured if all periodic layers in the slab have the same 2D periodicity. In this way one obtains closed-form expressions for the Q matrices of the composite structure, which contain the complex transmission and reflection coefficients of the slab and essentially define the so-called scattering S matrix [4–6]. It is then straightforward to evaluate the transmittance, $\mathcal{T}$, and the reflectance, $\mathcal{R}$, of the given slab by the ratio of the transmitted or reflected energy flux to the energy flux associated with the incident wave. The corresponding extinction is given, as usual, by the negative natural logarithm of the transmittance. If lossy materials are present, the absorbance, $\mathcal{A}$, of the slab is calculated from energy conservation: $\mathcal{A}=1-\mathcal{T}-\mathcal{R}$. On the other hand, the possible eigenmodes of the slab are obtained by requiring existence of a wave field localized within the slab in the absence of incident wave. Dividing the slab into a left and a right part, described by reflection matrices $\mathbf{Q}_{\mathrm{L}}^{\mathrm{II}}$ and $\mathbf{Q}_{\mathrm{R}}^{\mathrm{III}}$, respectively, this requirement leads to the secular equation [32,33]

$$\det[\mathbf{I}-\mathbf{Q}_{\mathrm{L}}^{\mathrm{II}}\mathbf{Q}_{\mathrm{R}}^{\mathrm{III}}]=0, \tag{10}$$

where $\mathbf{I}$ is the unit matrix.

For a 3D photonic crystal consisting of an infinite periodic sequence of layers stacked along the z-direction, the wave field in the host region between the n-th and the $(n+1)$-th unit slab has the form $\mathbf{E}(\mathbf{r})=\sum_{\mathbf{g}p}\{E^{+}_{\mathbf{g}p;n}\exp[i\mathbf{K}^{+}_{\mathbf{g}}\cdot(\mathbf{r}-\mathbf{A}_n)]+E^{-}_{\mathbf{g}p;n}\exp[i\mathbf{K}^{-}_{\mathbf{g}}\cdot(\mathbf{r}-\mathbf{A}_n)]\}\hat{\mathbf{e}}_p$, where $\mathbf{A}_n$ is an appropriate origin between the n-th and the $(n+1)$-th slab. The coefficients $E^{\pm}_{\mathbf{g}p;n}$ are obviously related to $E^{\pm}_{\mathbf{g}p;n+1}$ through the Q matrices of the unit slab. In matrix form we have

$$\begin{aligned}\mathbf{E}^{+}_{n+1}&=\mathbf{Q}^{\mathrm{I}}\mathbf{E}^{+}_{n}+\mathbf{Q}^{\mathrm{II}}\mathbf{E}^{-}_{n+1}\\ \mathbf{E}^{-}_{n}&=\mathbf{Q}^{\mathrm{III}}\mathbf{E}^{+}_{n}+\mathbf{Q}^{\mathrm{IV}}\mathbf{E}^{-}_{n+1}.\end{aligned} \tag{11}$$

On the other hand, Bloch's theorem implies that $\mathbf{E}^{\pm}_{\mathbf{g}p;n+1}=\exp(i\mathbf{k}\cdot\mathbf{a}_3)\mathbf{E}^{\pm}_{\mathbf{g}p;n}$, where $\mathbf{a}_3$ is a vector which connects a point in the n-th slab to an equivalent point in the $(n+1)$-th slab and $\mathbf{k}=(\mathbf{k}_\parallel,k_z(\omega,\mathbf{k}_\parallel))$. For given ω and $\mathbf{k}_\parallel$ one can obtain k_z from the following eigenvalue equation:

$$\begin{aligned}&\begin{pmatrix}\mathbf{Q}^{\mathrm{I}} & \mathbf{Q}^{\mathrm{II}}\\ -[\mathbf{Q}^{\mathrm{IV}}]^{-1}\mathbf{Q}^{\mathrm{III}}\mathbf{Q}^{\mathrm{I}} & [\mathbf{Q}^{\mathrm{IV}}]^{-1}[\mathbf{I}-\mathbf{Q}^{\mathrm{III}}\mathbf{Q}^{\mathrm{II}}]\end{pmatrix}\begin{pmatrix}\mathbf{E}^{+}_{n}\\ \mathbf{E}^{-}_{n+1}\end{pmatrix}\\ &\quad=\exp(i\mathbf{k}\cdot\mathbf{a}_3)\begin{pmatrix}\mathbf{E}^{+}_{n}\\ \mathbf{E}^{-}_{n+1}\end{pmatrix},\end{aligned} \tag{12}$$

which follows directly from Eq. (11) and Bloch's theorem. Alternatively, one can formulate an eigenvalue equation for the transfer matrix

$$\begin{aligned}&\begin{pmatrix}\mathbf{Q}^{\mathrm{I}}-\mathbf{Q}^{\mathrm{II}}[\mathbf{Q}^{\mathrm{IV}}]^{-1}\mathbf{Q}^{\mathrm{III}} & \mathbf{Q}^{\mathrm{II}}[\mathbf{Q}^{\mathrm{IV}}]^{-1}\\ -[\mathbf{Q}^{\mathrm{IV}}]^{-1}\mathbf{Q}^{\mathrm{III}} & [\mathbf{Q}^{\mathrm{IV}}]^{-1}\end{pmatrix}\begin{pmatrix}\mathbf{E}^{+}_{n}\\ \mathbf{E}^{-}_{n}\end{pmatrix}\\ &\quad=\exp(i\mathbf{k}\cdot\mathbf{a}_3)\begin{pmatrix}\mathbf{E}^{+}_{n}\\ \mathbf{E}^{-}_{n}\end{pmatrix}.\end{aligned} \tag{13}$$

The solutions $k_z(\omega,\mathbf{k}_\parallel)$ resulting from Eq. (12), or equivalently Eq. (13), looked upon as functions of real ω, define for each $\mathbf{k}_\parallel$ lines in the complex k_z plane, which all together constitute the complex band structure of the infinite crystal associated with the given crystallographic plane. A line of given $\mathbf{k}_\parallel$ may be real (in the sense that k_z is real) over certain frequency regions, and be complex (in the sense that k_z is complex) for ω outside these regions. It turns out that for given $\mathbf{k}_\parallel$ and ω, out of the solutions $k_z(\omega,\mathbf{k}_\parallel)$, none or, at best, a few are real and the corresponding eigenvectors represent propagating modes of the EM field in the given infinite crystal. The remaining solutions $k_z(\omega,\mathbf{k}_\parallel)$ are complex and the corresponding eigenvectors represent evanescent waves. These have an amplitude which increases exponentially in the positive or negative z-direction and, unlike the propagating waves, do not exist as physical entities in the infinite crystal. However, they are an essential part of the physical solutions of the EM field in the case of a surface or a slab of finite thickness. A region of frequency where propagating waves do not exist, for given $\mathbf{k}_\parallel$, constitutes a frequency gap of the EM field for the given $\mathbf{k}_\parallel$. If over a frequency region no propagating wave exists whatever the value of $\mathbf{k}_\parallel$, then this region constitutes an absolute frequency gap.

The transfer matrix on the left-hand side of Eq. (13) can also provide the reflection matrix, $\mathbf{R}_\infty$, of the corresponding semi-infinite crystal. Moreover, through $\mathbf{R}_\infty$ one can find the surface states of the crystal, if such exist. In order to obtain $\mathbf{R}_\infty$, the eigenvectors of the transfer matrix need to be arranged in a matrix $\mathbf{F}$ which projects the space of forward and backward Bloch eigenmodes, $\mathbf{V}^{+}$ and $\mathbf{V}^{-}$, onto the original plane-wave basis, as follows [7,34]:

$$\begin{pmatrix}\mathbf{E}^{+}_{0}\\ \mathbf{E}^{-}_{0}\end{pmatrix}=\begin{pmatrix}\mathbf{F}^{++} & \mathbf{F}^{+-}\\ \mathbf{F}^{-+} & \mathbf{F}^{--}\end{pmatrix}\begin{pmatrix}\mathbf{V}^{+}\\ \mathbf{V}^{-}\end{pmatrix}. \tag{14}$$

By definition, each eigenmode propagates through the crystal without changing its state and, on the other hand, for a semi-infinite crystal, there is no rear surface to reflect the forward into backward Bloch waves. Therefore, the appropriate boundary condition for the scattering problem of an EM wave incident on a semi-infinite photonic crystal from the homogeneous host material that extends to infinity is $\mathbf{V}^{-}=\mathbf{0}$ [34]. Then Eq. (14) yields

$$\mathbf{E}^{-}_{0}=\mathbf{F}^{-+}[\mathbf{F}^{++}]^{-1}\mathbf{E}^{+}_{0}\equiv\mathbf{R}_\infty\mathbf{E}^{+}_{0}. \tag{15}$$

On the other hand, the condition for the occurrence of surface states translates to the existence of non-zero forward Bloch modes ($\mathbf{V}^{+}\neq\mathbf{0}$) in the absence of incoming field ($\mathbf{E}^{+}_{0}=\mathbf{0}$) [10,35]. Then Eq. (14) gives $\mathbf{F}^{++}\mathbf{V}^{+}\equiv\mathbf{E}^{+}_{0}=\mathbf{0}$, which is satisfied when

$$\det[\mathbf{F}^{++}]=0. \tag{16}$$

3. Nonreciprocal planar magnetoplasmonic nanostructures

Plasmonic nanostructures can exhibit a substantial magneto-optical activity due to the excitation of localized surface plasmon resonance modes [36]. Compared to a

homogeneous plasma surface, discontinuous surfaces consisting of plasma nanoparticles provide a more flexible platform for tailoring plasmons by varying the shape and geometrical arrangement of the particles as well as their dielectric environment. As an example we consider an fcc crystal of plasma nanospheres, characterized by a relative magnetic permeability $\mu_p = 1$ and by the Drude relative electric permittivity [37]

$$\varepsilon_p = 1 - \frac{\omega_p^2}{\omega^2[1 + i/(\tau\omega)]}, \tag{17}$$

where τ is the relaxation time of the free carriers and ω_p is the bulk plasma frequency: $\omega_p^2 = ne^2/(m\varepsilon_0)$, with n, $-e$ and m being the carrier density, charge and mass, respectively. In what follows, we use ω_p as the frequency unit, which naturally introduces c/ω_p as the length unit. For the crystal under consideration we take the sphere radius $S = c/\omega_p$ and the nearest neighbor distance in the fcc lattice $a_0 = 2.2c/\omega_p$. We note that, assuming $\hbar\omega_p \simeq 10$ eV, which is a typical value for metals, c/ω_p corresponds to about 20 nm. For semiconductors, on the other hand, whose carrier densities can be easily varied within a broad range of values, but are always much lower than those in metals, the plasma frequency is much smaller (typically at mid- and far-infrared frequencies) and the length unit c/ω_p increases accordingly.

In the presence of a static uniform magnetic field, $\mathbf{B}$, the response of a plasma to a time-harmonic EM wave of angular frequency ω and electric-field component $\mathbf{E} = \mathbf{E}_0 \exp(-i\omega t)$, is described by the equation of motion of the electrons: $m\ddot{\mathbf{r}} = -m\tau^{-1}\dot{\mathbf{r}} - e\mathbf{E} - e\dot{\mathbf{r}} \times \mathbf{B}$. The resulting polarization density, $\mathbf{P} = -ne\mathbf{r}$, defines an electric displacement vector, $\mathbf{D} = \varepsilon_0\mathbf{E} + \mathbf{P}$, and finally yields the relative electric permittivity tensor $\overleftrightarrow{\varepsilon}_g$ of the magnetized plasma through $\mathbf{D} = \varepsilon_0\overleftrightarrow{\varepsilon}_g\mathbf{E}$. If we take $\mathbf{B}$ to be oriented along the z-direction, after some straightforward algebra we find that $\overleftrightarrow{\varepsilon}_g$ has the gyrotropic form of Eq. (1) with $\varepsilon_r = 1 - \omega_p^2\xi/(\omega^2\xi^2 - \omega_c^2)$, $\varepsilon_z = \varepsilon_p$, and $\varepsilon_\kappa = -\omega_c\omega_p^2/[\omega(\omega^2\xi^2 - \omega_c^2)]$. In these expressions, $\omega_c = eB/m$ is the cyclotron resonance frequency and $\xi = 1 + i/(\tau\omega)$. We note that, by setting $\omega_c = 0$, $\overleftrightarrow{\varepsilon}_g$ becomes a diagonal tensor with all of its diagonal elements equal to ε_p, as expected. In our calculations we shall neglect dissipative losses ($\tau^{-1} = 0$) for simplicity.

It has been recently shown that the fcc crystal of plasma nanospheres under consideration, in the absence of external magnetic field, supports surface, so-called Tamm, states at its (001) surface [10], which satisfy the reciprocity condition $\omega(-\mathbf{k}_\parallel) = \omega(\mathbf{k}_\parallel)$. We now apply a static uniform magnetic field parallel to the surface, along the y-direction, corresponding to $\omega_c = 0.01\omega_p$. This value of ω_c, though it is by an order of magnitude smaller than that considered by Yu et al. [38], corresponds to a prohibitively strong magnetic field, of the order of 10^3 T in the case of metals. For semiconductors however, the field becomes much weaker, of the order of 1 T or less. It is worth noting that if the spheres are magnetized in the z-direction the T matrix has a block diagonal form: $T_{Plm;P'l'm'} = T^{(m)}_{Pl;P'l'}\delta_{mm'}$. Moreover, $T^{(m)}_{Pl;P'l'}$ vanishes identically if the magnetic/electric multipoles corresponding to Pl and $P'l'$ do not have the same parity, even or odd, which means that the T matrix in a given m subspace is further reduced into two submatrices [12–14]. The above symmetry properties, however, do not hold in any coordinate system. In general, if α, β, γ are the Euler angles transforming an arbitrarily chosen coordinate system into the coordinate system in which the magnetization is oriented along the z-axis, the T matrix is given by

$$T_{Plm;P'l'm'} = \sum_{m''} D^{(l)}_{mm''}(\alpha,\beta,\gamma) T^{(m'')}_{Pl;P'l'} D^{(l')}_{m''m'}(-\gamma,-\beta,-\alpha), \tag{18}$$

where $D^{(l)}$ are the appropriate transformation matrices associated with the l irreducible representation of the $O(3)$ group [39]. Since in our case the static magnetic field is not oriented along the z-direction, which is by definition the direction of growth of the crystal in the LMS method, but along the y-direction, we need to transform the T matrix according to Eq. (18) using the appropriate Euler angles: $\alpha = 90^\circ$, $\beta = 90^\circ$, $\gamma = 0^\circ$.

In Fig. 4 we display the dispersion diagram, along the k_x-direction, of the optical Tamm states of the given crystal of plasma spheres, magnetized in the y-direction. The shaded regions in Fig. 4 represent frequency bands, i.e., at any frequency within a shaded region, for given $\mathbf{k}_\parallel = (k_x, 0)$, there exists at least one propagating EM mode in the infinite crystal. The blank regions represent frequency gaps and the dotted straight line denotes the light cone in the air host. With solid lines we show the dispersion of surface states, calculated according to Eq. (16), which lie, indeed, in gap regions and outside the light cone, i.e., they are true surface states since they decay exponentially in the crystal as well as in the outer region. As can be seen from the enlarged view of the dispersion curves in Fig. 4, the propagation of the surface states along the direction normal to the magnetic field changes and becomes nonreciprocal: $\omega(-k_x) \neq \omega(k_x)$. Reversal of the magnetic field direction has the same effect as reversal of the propagation direction ($k_x \to -k_x$) while, if the

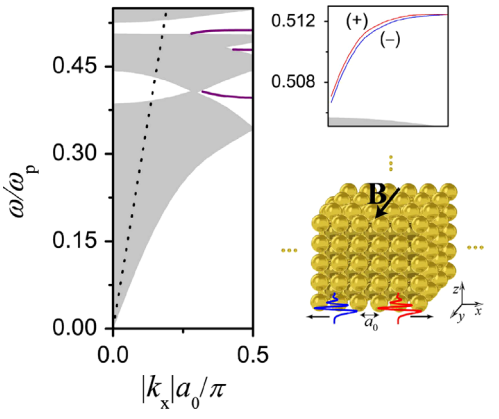

Fig. 4. Left-hand panel: Projection on the k_x-direction of the photonic band structure of an fcc crystal of Drude spheres (nearest neighbor distance: $a_0 = 2.2c/\omega_p$; sphere radius: $S = c/\omega_p$), grown along its [001] direction, under the action of a static uniform magnetic field corresponding to $\omega_c = 0.01\omega_p$ applied along the y-axis. Shaded and blank regions represent frequency bands and gaps, respectively. With solid lines in gap regions we show the dispersion curves of the surface states. The dotted line denotes the light cone in the host medium (air). Right-hand panel: An enlarged view of dispersion curves, with the (+) and (−) signs denoting positive and negative values of k_x, respectively, and a schematic representation of the crystal and its surface states.

magnetic field is perpendicular to the surface or parallel to the propagation direction, nonreciprocity is not encountered. This can be explained as follows. The structure under consideration is invariant under the C_{4v} point symmetry group [39]. If an external magnetic field is applied along the z-direction, i.e., perpendicular to the surface, the point group is reduced to C_4 since $\mathbf{P}\overleftrightarrow{\varepsilon}_g\mathbf{P}^{-1}=\overleftrightarrow{\varepsilon}_g$ only for those operations $\widehat{\mathbf{P}}$ of C_{4v} that belong to C_4, and spectral reciprocity $\omega(-\mathbf{k}_{\parallel})=\omega(\mathbf{k}_{\parallel})$ is always ensured by a rotation through an angle π about the z-axis, which is a symmetry operation of C_4. If now the magnetic field is in-plane, say along the y-direction, the relevant point symmetry group, C_{1h}, consists of two operations: Identity and reflection with respect to the $x-z$ plane [39]. Therefore, while reciprocity along the y-direction, $\omega(-k_y)=\omega(k_y)$, is ensured by mirror symmetry with respect to the $x-z$ plane, $\omega(-k_x)\neq\omega(k_x)$ because there is no group symmetry operation which transforms $(k_x,0,0)$ into $(-k_x,0,0)$, given also the lack of time-reversal symmetry. Consequently, nonreciprocity occurs for an in-plane external magnetic field in the Voigt (Cotton-Mouton) geometry, i.e., when light propagates perpendicular to the magnetic field. As a result of the spectral splitting of the dispersion curves associated with the forward and backward propagating waves, within a short frequency range near their band edges, only modes propagating in one direction exist. The relative spectral shift of the bands depends on the magnitude of the external field, which allows for the design of tunable surface states for one-way light transport. A similar nonreciprocal behavior has been reported for surface modes at truncated one-dimensional magnetophotonic crystals [40].

An alternative design, which enables to overcome the major drawback of the previous nonreciprocal structure, namely, the need for a strong external magnetic field, may consist of a layer of magnetic garnet particles on top of the surface of a homogeneous plasmonic material. In this case, nonreciprocity is introduced by the magneto-optic properties of the garnet material [41] that can be magnetically saturated by relatively weak magnetic fields. It should be noted that, even though the same effect can be obtained using a uniform gyrotropic overlayer, particle arrays offer additional flexibility for optimization of the design by properly adjusting the different geometric parameters involved, such as particle size and shape, and interparticle distance. We consider a 2D array of garnet spheres on top of the surface of a homogeneous plasmonic material, described by the Drude relative electric permittivity of Eq. (17) neglecting dissipative losses. The spheres have a radius $S=c/\omega_p$ and are arranged on a square lattice of lattice constant $a_0=2.2c/\omega_p$. The optical response of the spheres, if they are magnetized along the z-direction, is described by a relative electric permittivity tensor of the form of Eq. (1) with $\varepsilon_r=\varepsilon_z=6.25$ and $\varepsilon_\kappa=0.06$, values which are appropriate for magnetic garnet materials [42–44]. In Fig. 5 we depict the dispersion diagram of the surface plasmon polariton modes in this structure, calculated according to Eq. (10) along the k_x-direction if the garnet spheres are magnetized in the y-direction. Because of the 2D periodicity of the coating layer, the dispersion curves are folded into the SBZ and Bragg gaps

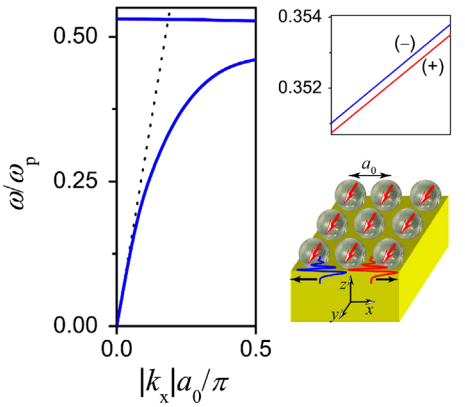

Fig. 5. Left-hand panel: Dispersion diagram in the k_x-direction of the plasmon modes at the surface of a homogeneous Drude material coated with a square array of garnet spheres (lattice constant: $a_0=2.2c/\omega_p$, sphere radius $S=c/\omega_p$) magnetized in the y-direction. The dotted line denotes the light cone in air. Right-hand panel: An enlarged view of the dispersion diagram, with the $(+)$ and $(-)$ signs denoting positive and negative values of k_x, respectively, and a schematic representation of the structure and the surface plasmon polariton modes.

open up at the Brillouin zone boundaries. Again, as can be seen from an enlarged view of the dispersion diagram, the propagation of the surface plasmon polariton modes along the direction normal to the magnetic field becomes nonreciprocal: $\omega(-k_x)\neq\omega(k_x)$.

4. Conclusion

In summary, we presented an extended version of the full-electrodynamic LMS method for photonic structures of particles of various kinds, emphasizing on gyrotropic spheres with arbitrarily oriented gyration vector. The applicability and efficiency of the method is demonstrated by two illustrative examples of surface geometries without inversion center, namely a semi-infinite fcc crystal of magnetized plasma nanospheres and a homogeneous plasma substrate covered by a square array of magnetic garnet nanospheres. Spectral nonreciprocity of photonic Tamm and surface plasmon polariton states, which emerges as a result of the simultaneous lack of space-inversion and time-reversal symmetries, is demonstrated in the Voigt configuration.

Acknowledgments

A. Christofi is supported by a SPIE Optics and Photonics Education Scholarship.

References

[1] Figotin A, Vitebsky I. Nonreciprocal magnetic photonic crystals. Phys Rev E 2001;63:066609.
[2] Armelles G, Cebollada A, García-Martín A, González MU. Magneto-plasmonics: combining magnetic and plasmonic functionalities. Adv Opt Mater 2013;1:10–35.
[3] Stefanou N, Modinos A. Scattering of light from a two-dimensional array of spherical particles on a substrate. J Phys: Condens Matter 1991;3:8135–48.

[4] Stefanou N, Yannopapas V, Modinos A. Heterostructures of photonic crystals: frequency bands and transmission coefficients. Comput Phys Commun 1998;113:49–77.
[5] Stefanou N, Yannopapas V, Modinos A. MULTEM 2: a new version of the program for transmission and band-structure calculations of photonic crystals. Comput Phys Commun 2000;132:189–96.
[6] Gantzounis G, Stefanou N. Layer-multiple-scattering method for photonic crystals of nonspherical particles. Phys Rev B 2006;73:035115.
[7] Tserkezis C, Stefanou N. Retrieving local effective constitutive parameters for anisotropic photonic crystals. Phys Rev B 2010;81:115112.
[8] Stefanou N, Tserkezis C, Gantzounis G. Plasmonic excitations in ordered assemblies of metallic nanoshells. Proc SPIE 2008;6989:698910.
[9] Christofi A, Stefanou N, Gantzounis G. Photonic eigenmodes and light propagation in periodic structures of chiral nanoparticles. Phys Rev B 2011;83:245126.
[10] Tserkezis C, Stefanou N, Gantzounis G, Papanikolaou N. Photonic surface states in plasmonic crystals of metallic nanoshells. Phys Rev B 2011;84:115455.
[11] Christofi A, Stefanou N. Photonic structures of metal-coated chiral spheres. J Opt Soc Am B 2012;29:1165–71.
[12] Lin Z, Chui ST. Electromagnetic scattering by optically anisotropic magnetic particle. Phys Rev E 2004;69:056614.
[13] Li LW, Ong WL. A new solution for characterizing electromagnetic scattering by gyroelectric sphere. IEEE Trans Antennas Propag 2011;59:3370.
[14] Li JLW, Ong WL, Zheng KHR. Anisotropic scattering effects of a gyrotropic sphere characterized using the T-matrix method. Phys Rev E 2012;85:036601.
[15] Bohren CF, Huffman DR. Absorption and scattering of light by small particles. New York: Wiley Interscience; 1998.
[16] Wu ZS, Wang YP. Electromagnetic scattering for multilayered sphere: recursive algorithms. Radio Sci 1991;26:1393–401.
[17] Sinzig J, Quinten M. Scattering and absorption by spherical multilayer particles. Appl Phys A 1994;58:157–62.
[18] Bohren CF. Light scattering by an optically active sphere. Chem Phys Lett 1974;29:458–62.
[19] Lakhtakia A, Varadan VK, Varadan VV. Scattering and absorption characteristics of lossy dielectric, chiral, nonspherical objects. Appl Opt 1985;24:4146–54.
[20] Psarobas IE, Stefanou N, Modinos A. Photonic crystals of chiral spheres. J Opt Soc Am A 1999;16:343–7.
[21] Wu ZS, Shang QC, Li ZJ. Calculation of electromagnetic scattering by a large chiral sphere. Appl Opt 2012;51:6661–8.
[22] Mishchenko MI, Travis LD, Lacis AA. Scattering, absorption, and emission of light by small particles. Cambridge: Cambridge University Press; 2002.
[23] Mishchenko MI. Light scattering by randomly oriented axially symmetric particles. J Opt Soc Am A 1991;6:871–82.
[24] Mishchenko MI, Hovenier JW, Travis LD, editors. Light scattering by nonspherical particles: theory, measurements, and applications. San Diego: Academic Press; 1999.
[25] Johnson BR. Invariant imbedding T-matrix approach to electromagnetic scattering. Appl Opt 1988;27:4861–73.
[26] Bi L, Yang P, Kattawar GW, Mishchenko MI. Efficient implementation of the invariant imbedding T-matrix method and the separation of variables method applied to large nonspherical inhomogeneous particles. J Quant Spectrosc Radiat Transf 2013;116:169–83.
[27] Bi L, Yang P, Kattawar GW, Mishchenko MI. A numerical combination of extended boundary condition method and invariant imbedding method applied to light scattering by large spheroids and cylinders. J Quant Spectrosc Radiat Transf 2013;123:17–22.
[28] Tserkezis C, Gantzounis G, Stefanou N. Collective plasmonic modes in ordered assemblies of metallic nanoshells. J Phys: Condens Matter 2008;20:075232.
[29] Pendry JB. Low energy electron diffraction: the theory and its applications to determination of surface structure. New York: Academic Press; 1974.
[30] Stokes GG. On the intensity of the light reflected from or transmitted through a pile of plates. Proc R Soc Lond 1860;11:545556.
[31] van de Hulst HC. A new look at multiple scattering. Technical Report, NASA Institute for Space Studies Goddard Space Flight Center, New York; 1963.
[32] Sainidou R, Stefanou N. Guided and quasiguided elastic waves in phononic crystal slabs. Phys Rev B 2006;73:184301.
[33] Stefanou N, Gantzounis G, Tserkezis C. Multiple-scattering calculations for plasmonic nanostructures. Int J Nanotechnol 2009;6:137–63.
[34] Li Z-Y, Ho K-M. Light propagation in semi-infinite photonic crystals and related waveguide structures. Phys Rev B 2003;68:155101.
[35] Lawrence FJ, Botten LC, Dossou KB, McPhedran RC, de Sterke CM. Photonic-crystal surface modes found from impedances. Phys Rev A 2010;82:053840.
[36] Sepúlveda B, González-Díaz JB, García-Martín A, Lechuga LM, Armelles G. Plasmon-induced magneto-optical activity in nanosized gold disks. Phys Rev Lett 2010;104:147401.
[37] Ashcroft NW, Mermin ND. Solid state physics. New York: Saunders; 1976.
[38] Yu Z, Veronis G, Wang Z, Fan S. One-way electromagnetic waveguide formed at the interface between a plasmonic metal under a static magnetic field and a photonic crystal. Phys Rev Lett 2008;100:23902.
[39] Inui T, Tanabe Y, Onodera Y. Group theory and its applications in physics. Berlin: Springer; 1990.
[40] Khanikaev AB, Baryshev AV, Inoue M, Kivshar YS. One-way electromagnetic Tamm states in magnetophotonic structures. Appl Phys Lett 2009;95:011101.
[41] Kuzmiak V, Eyderman S, Vanwolleghem M. Controlling surface plasmon polaritons by a static and/or time-dependent external magnetic field. Phys Rev B 2012;86:045403.
[42] Drezdzon SM, Yoshie T. On-chip waveguide isolator based on bismuth iron garnet operating via nonreciprocal single-mode cutoff. Opt Express 2009;17:9276–81.
[43] Khanikaev AB, Mousavi SH, Shvets G, Kivshar YS. One-way extraordinary optical transmission and nonreciprocal spoof plasmons. Phys Rev Lett 2010;105:126804.
[44] Fang K, Yu Z, Liu V, Fan S. Ultracompact nonreciprocal optical isolator based on guided resonance in a magneto-optical photonic crystal slab. Opt Lett 2009;36:4254–6.